THE GEOLOGICAL SOCIETY OF AMERICA®

Iron microbialites from an acidic Martian analog (Río Tinto, Spain)—Implications for finding life on Mars

Yu Pei[1,2,†], Muammar Mansor[2], Philip Werner[2,3], Jeremiah Shuster[2,4], Eric Runge[2,5], Prachi Joshi[2,6], Ronny Schoenberg[2], Ricardo Amils[7,8], Cristina Escudero[2], Walter Goetz[9], Andreas Kappler[2], and Jan-Peter Duda[2,5,†]

[1]*State Key Laboratory of Geomicrobiology and Environmental Changes, Hubei Key Laboratory of Planetary Geology and Deep-Space Exploration, China University of Geosciences (Wuhan), Wuhan, Hubei 430074, China*
[2]*Department of Geosciences, University of Tübingen, 72076 Tübingen, Baden-Württemberg, Germany*
[3]*Institute of Earth Surface Dynamics, University of Lausanne, Lausanne, Vaud 1015, Switzerland*
[4]*Department of Earth Sciences, Western University, London, Ontario N6A 3K7, Canada*
[5]*Department of Geobiology, Geoscience Center, University of Göttingen, 37077 Göttingen, Niedersachsen, Germany*
[6]*Forest Soils and Biogeochemistry, Swiss Federal Institute for Forest, Snow and Landscape Research WSL, Birmensdorf, Zürich CH-8903, Switzerland*
[7]*Centro de Astrobiología, Madrid 28850, Spain*
[8]*Centro de Biología Molecular Severo Ochoa, Universidad Autónoma de Madrid, Madrid 28049, Spain*
[9]*Max Planck Institute for Solar System Research, 37077 Göttingen, Niedersachsen, Germany*

ABSTRACT

The search for life on Mars requires identifying suitable biosignatures detectable by rover missions or in returned samples. To support the progressing astrobiological exploration of Mars, we investigated modern iron microbialites from Río Tinto, Spain, an acidic terrestrial analog to the Meridiani Planum. We used an integrative approach combining a suite of tools (Raman and Mössbauer spectroscopy, micro X-ray diffraction [μXRD], micro X-ray fluorescence [μXRF]) analogous to the instruments onboard various Mars rovers. Our analyses revealed that the ~10-cm-thick microbialites exhibit alternating porous and dense layers of jarosite and Fe(III) (oxyhydr)oxides, locally common minerals on Mars. The estimated growth rate of the layered structures (1 mm per year) is very high considering the slow precipitation kinetics of the constituent minerals, inconsistent with solely abiotic precipitation. $\delta^{56}Fe$ data for the different layers (−0.91‰ to −0.83‰) and calculated isotopic differences ($\Delta^{56}Fe_{(III)solid\text{-}aq}$ = −0.62‰ to −0.54‰) were consistent with both biotic and abiotic mineral precipitation. Scanning electron microscope–energy-dispersive X-ray spectroscopy (SEM-EDS) and DNA analyses confirmed the presence of microorganisms known for promoting iron mineral formation, including archaea (e.g., Thermoplasmata) and bacteria (e.g., *Acidithiobacillus*). Our study highlights three lines of biogenicity: (1) non-isopachous layered structures, (2) high growth rate, and (3) the presence of microorganisms that likely promote iron mineral precipitation. Problematically, growth rates and the presence of relevant microorganisms cannot be reliably inferred or detected, either in the geological record or by the rovers, while layered structures can also form abiotically. While highlighting such challenges in interpreting iron microbialites in modern systems, our study provides a robust framework for exploring these structures on ancient Earth. It also underscores the critical role of integrating high-confidence morphological and geochemical biosignatures—ideally from sample return missions—in the search for life on Mars.

INTRODUCTION

Microbialites (i.e., deposits formed by benthic microbial communities; Burne and Moore, 1987) provide a wealth of textural, mineralogical, and (bio)geochemical information about the processes involved in their formation. Microbialites are among the earliest evidence of life on Earth, with the first undisputed occurrences on Earth dating back to ca. 3.5–3.4 Ga (Tice and Lowe, 2004; Van Kranendonk, 2011; Duda et al., 2016; Lepot, 2020; Reinhardt et al., 2024; Weimann et al., 2024). Considering that the earliest microbialites in the terrestrial rock record are broadly contemporaneous with the expected early window of habitability on Mars (Bibring et al., 2006), microbialites (including microbially induced sedimentary structures, MISS) could be promising targets in the search for life on Mars (Westall et al., 2015; Hays et al., 2017; Noffke, 2021; Hickman-Lewis et al., 2023).

Research has primarily focused on carbonate-dominated microbialites as these are the most widespread in the geological record (Arp et al., 2001; Suarez-Gonzalez et al., 2019; Pei et al., 2024). Microbialites consisting of various Fe(III) (oxyhydr)oxides, hereafter referred to as "iron microbialites," are important because they have been reported from a variety of marine and non-marine circumneutral pH environments on Earth, ranging from the Paleoproterozoic to the Cenozoic (Planavsky et al., 2009; Champenois et al., 2024). Since Fe(III) (oxyhydr)oxides are widespread on the Martian surface (Ehlmann and Edwards, 2014; Kaplan et al., 2016; Hurowitz et al., 2017; Fraeman et al., 2020; Hazen et al., 2023; Valantinas et al., 2025), ancient aquatic deposits on the red planet could have preserved iron microbialites. However, the biosignature potential of iron microbialites is limited, as the formation and preservation of such deposits on Earth is poorly understood.

Jan-Peter Duda https://orcid.org/0000-0002-8959-097X
†Y. Pei, peiyu@cug.edu.cn; J.-P. Duda, jan-peter.duda@uni-goettingen.de

GSA Bulletin;
Published online 24 June 2026

https://doi.org/10.1130/B38599.1.

© 2026 The Authors. Gold Open Access:
This paper is published under the terms of the CC-BY license.

Downloaded from http://pubs.geoscienceworld.org/gsa/gsabulletin/article-pdf/doi/10.1130/B38599.1/8045496/b38599.pdf by Universitaetsbibliothek Tuebingen user on 25

The extremely acidic (pH: ~2) aquatic environments of Río Tinto, Spain, share remarkable mineralogical and geochemical similarities to Meridiani Planum on Mars (e.g., the presence of jarosite [$KFe_3(SO_4)_2(OH)_6$] formed in a wet, oxidizing, and acidic environment) and can, therefore, be considered a modern terrestrial analog (Morris et al., 2006; Amils et al., 2014; Kaplan et al., 2016). The highly acidic and heavy-metal-enriched surface water in Río Tinto has resulted from the biologically driven oxidation of ca. 350 Ma massive iron sulfide deposits in the subsurface as well as microbial $Fe^{2+}_{(aq)}$ oxidation (Amils et al., 2014, 2023; Abramov et al., 2022). In the associated surface environment, acidophilic microorganisms, including Fe(II)-oxidizing bacteria (e.g., *Acidithiobacillus*, *Leptospirillum*) and fungi (e.g., *Purpureocillium lilacinum*) are known to promote the formation of jarosite, schwertmannite [$Fe_8O_8(OH)_{8-2x}(SO_4)_x \times nH_2O$, where $1 < x < 1.75$], and Fe(III) (oxyhydr) oxides such as goethite (α-FeOOH; Oggerin et al., 2016; Abramov et al., 2022). These processes result in the local formation of distinct biosedimentary deposits, such as terraced iron formations (Sánchez España et al., 2007).

Here, we investigate iron microbialites from the Río Tinto area to support the astrobiological exploration of Mars (Fig. 1A). Our study integrates data from analytical instruments analogous to those used in Mars rover missions (Raman and Mössbauer spectroscopy; micro X-ray diffraction [μXRD]; micro X-ray fluorescence [μXRF]) with data from Earth-based analytical methods relevant to sample return missions (e.g., scanning electron microscope coupled with energy-dispersive X-ray spectroscopy [SEM-EDS]; δ^{56}Fe isotopes; 16S rRNA). We investigate the mechanisms involved in microbialite formation before focusing on the value of observed physicochemical features as potential biosignatures for Mars. Taken together, the findings of our study provide a robust framework for exploring iron microbialites on ancient Earth and support our search for life on Mars.

FIELD OBSERVATION AND SAMPLING

The iron microbialites grew horizontally on the northeast-facing wall of an ~100-year-old water reservoir (several hundred square meters in size; 37°43′17.3″N, 6°33′46.7″W), close to the Río Tinto's origin (Figs. 1A and 1B). Between 2008 and 2022, the average pH of the reservoir water was 2.3 ± 0.3 ($n = 22$). Several iron microbialites were sampled during two field campaigns in September 2021 and 2022. Following established practice in microbialite research, we selected one representative microbialite collected in 2021 for petrographic, mineralogical, and geochemical analyses; only 16S rRNA analyses were conducted on two additional microbialites collected in 2022 to ensure reproducibility.

METHODS

Petrographic Analyses

Petrographic thin sections of the microbialites were analyzed using a Keyence VHX-6000 digital microscope. For SEM-EDS analysis, a Crossbeam 550L SEM (Zeiss; Oberkochen, Germany) was used. Samples were fixed in 2.5% glutaraldehyde in the field and immediately stored at 4 °C. This treatment promoted cross-linking of cellular macromolecules, resulting in stabilization of cellular architecture, preservation of ultrastructural integrity, and inhibition of biological activity. In the laboratory, the samples were dehydrated with different concentrations of ethanol (25%, 50%, 75%, and 100% in turn) and then dried onto carbon adhesive tabs attached to aluminum stubs. The sequential use of increasing ethanol concentrations ensured gradual replacement of intracellular water, thereby minimizing osmotic stress and preventing structural collapse. This gentle dehydration procedure was critical for maintaining morphological fidelity during subsequent drying and vacuum imaging, thereby ensuring high-resolution preservation of microbial ultrastructure. The dried samples mounted on carbon adhesive tabs were coated with 28-nm-thick layers of gold using a BALTEC SCD 005 sputter coater to reduce charging effects. Images were collected at a working distance of ~5 mm and a voltage of 2 kV.

μXRD was performed on powdered samples using a Bruker's D8 Discover GADDS XRD^2 instrument equipped with a standard sealed tube and a copper anode (30 kV/30 mA). The measuring time was 240 seconds at two detector positions (15° and 40°). Phases were identified by using Match! software combined with the Crystallography Open Database (COD-Inorg REV211633 2022.06.29).

For Mössbauer spectroscopy, powdered samples were loaded into Plexiglas holders (area 1 cm^2), forming a disc. The holders were inserted into a closed-cycle exchange gas cryostat (Janis cryogenics) under a backflow of helium to minimize exposure to air. Spectra were collected at 77 K, 295 K, and 5 K. A constant acceleration drive system (WissEl) in transmission mode with a ^{57}Co/Rh source was used. All spectra were calibrated against a 7-μm-thick α-^{57}Fe foil that was measured at room temperature. Mössbauer spectra analysis was carried out using Recoil (University of Ottawa, Ontario, Canada) and the extended Voigt Based Fitting (VBF) routine (Lagarec and Rancourt, 1997).

Element distribution images of thin sections were obtained by using a μXRF M4 Tornado spectrometer (Bruker Nano GmbH; Berlin, Germany). Measurements (spatial resolution = 20 μm, pixel time = 18 ms) were conducted at 25 kV and 600 nA.

A WITec alpha300 R fiber-coupled ultra-high throughput spectrometer was employed to collect Raman single spectra to determine mineral compositions of thin sections. Before analysis, the system was calibrated employing an integrated light source. For single spectra, the experimental setup included a 532-nm continuous-wave excitation laser, an automatically controlled laser power of 2 mW, a 100×-long working distance objective with a numerical aperture of 0.75, and a 300-g mm^{-1} grating. The spectrometer was centered at 2200 rel. cm^{-1}, covering a spectral range from 68 rel. cm^{-1} to 3914 rel. cm^{-1}. This setup has a spectral resolution of 2.2 cm^{-1}. For single spectra, each was collected by two accumulations, with an acquisition time of 20 s. Automated cosmic ray correction, background subtraction, and fitting using a Lorentz function were performed using the WITec Project software.

Bulk Analyses

Total organic carbon (TOC) contents were analyzed with a TOC analyzer (Analytics; Jena, Germany). Each powdered sample was individually heated up to a maximum temperature of 900 °C. At 400 °C, TOC was released, while residual organic carbon (ROC) and total inorganic carbon (TIC) were released at 600 °C and at 900 °C, respectively. ROC and TIC were below detection limit for all analyzed samples.

DNA Analyses

Total DNA was extracted from internal and external layers of two different microbialites stored at −20 °C according to the method of Lueders et al. (2004). Microbial 16S rRNA genes were amplified using primers 515F and 806R targeting the V4 region (Caporaso et al., 2010). Real-time quantitative polymerase chain reaction (qPCR) was used to quantify general 16S rRNA genes of bacteria and archaea. The qPCR protocol was performed using a CFX96 real-time PCR system (Bio-Rad). Subsequent Illumina sequencing was performed at the Next Generation Sequencing Competence Center Tübingen (NCCT) in Germany and between 85,213 and 160,167 read pairs were obtained for each sample.

Sequencing data was processed using nf-core/ampliseq version 2.8.0 (Straub et al., 2020) from the nf-core collection of workflows (Ewels et al., 2016), utilizing reproducible software environ-

Downloaded from http://pubs.geoscienceworld.org/gsa/gsabulletin/article-pdf/doi/10.1130/B38599.1/8045496/b38599.pdf by Universitaetsbibliothek Tuebingen user on 25

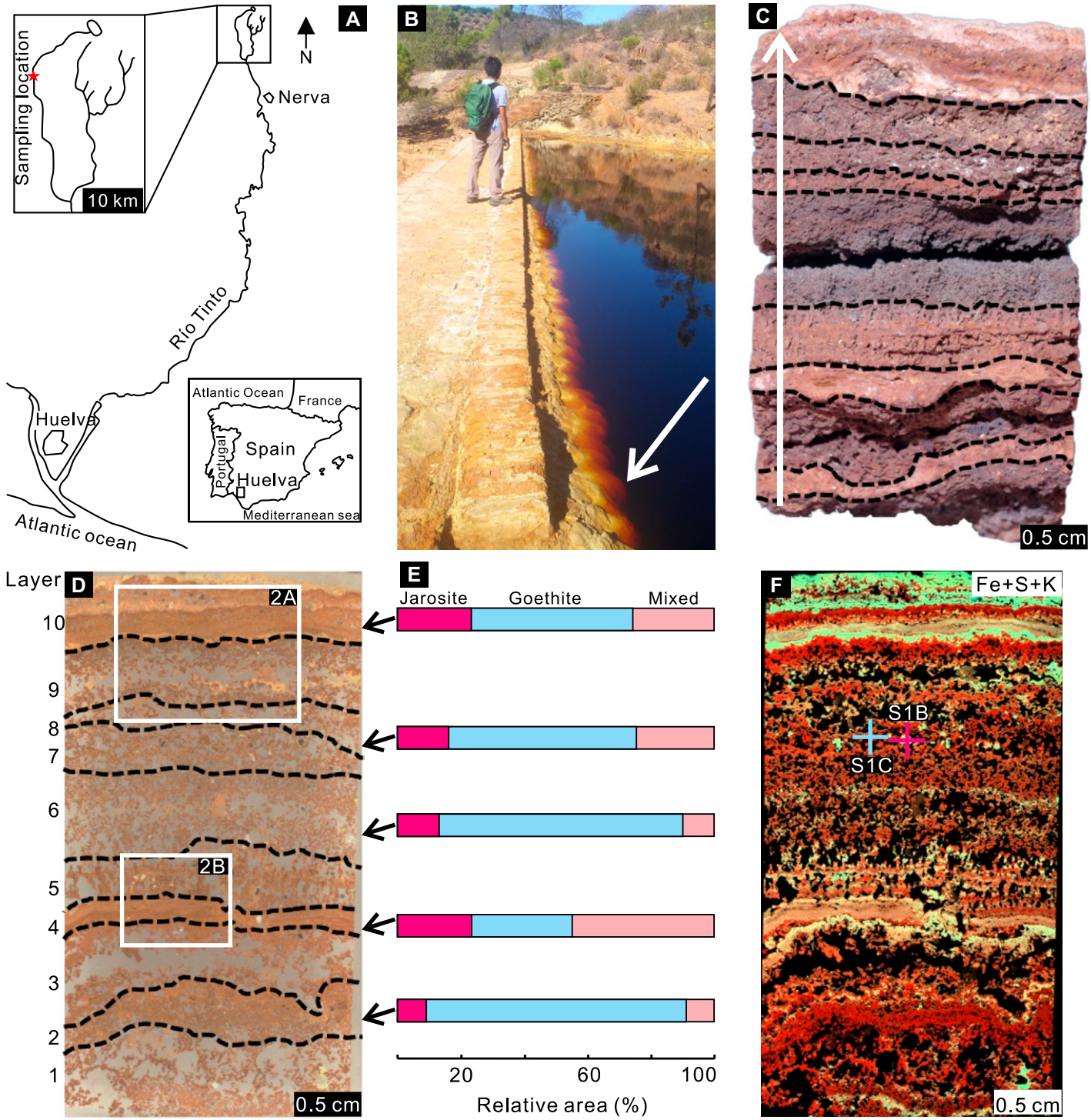

Figure 1. (A) Sampling location at the origin of Río Tinto, Spain (modified from García-Moyano et al., 2007). (B) The iron microbialites (white arrow) grew horizontally on a northeast-facing wall. (C, D) The analyzed iron microbialite was ~10 cm thick and consisted of ~1-cm-thick layers of alternating color and texture. (E) Mössbauer spectroscopy indicated the presence of jarosite and Fe(III) (oxyhydr) oxides, including goethite, in the iron microbialites. (F) Micro X-ray fluorescence (μXRF) analysis revealed relative enrichments of Fe (red), S (yellow), and K (cyan) in dense layers as compared to porous layers.

ments from the Bioconda (Grüning et al., 2018) and BioContainers (da Veiga Leprevost et al., 2017) projects.

Data quality was evaluated with FastQC version 0.12.1 (Andrews, 2010) and summarized with MultiQC version 1.23 (Ewels et al., 2016). Cutadapt 3.4 (Martin, 2011) was used to trim primers, discarding all untrimmed sequences. Sequences lacking primer sequences were con-

Downloaded from http://pubs.geoscienceworld.org/gsa/gsabulletin/article-pdf/doi/10.1130/B38599.1/8045496/b38599.pdf by Universitaetsbibliothek Tuebingen user on 25

sidered artifacts. Less than 17.8% of sequences were discarded per sample, with a mean of 88.7% of sequences per sample passing the filtering. Adapter and primer-free sequences were processed as one pool using DADA2 version 4.3.1 (Callahan et al., 2016) to eliminate PhiX contamination, trim reads, discard reads with >2 expected errors, correct errors, merge read pairs, and remove PCR chimeras. Ultimately, 396 amplicon sequence variants (ASVs) were obtained across all samples, with 70.3% to 78.26% of reads per sample (average 75.9%) retained. The ASV count table contained a total of 370,984 counts, with at least 49,242 and at most 109,678 per sample (average 92,746). ASVs with lengths <250 bp or >260 bp were removed, affecting less than 2.17% of counts per sample, resulting in 375 ASVs passing.

Taxonomic classification was performed using DADA2 and the Silva 138.1 prokaryotic SSU database (Quast et al., 2013). ASV sequences, abundances, and DADA2 taxonomic assignments were loaded into QIIME 2 (Bolyen et al., 2019). Of the 375 ASVs, 34 were filtered out using taxonomic strings containing "mitochondria" or "chloroplast," leaving 341 ASVs. Within QIIME 2, the final prokaryotic community data was visualized in a bar plot, evaluated for sufficient sequencing depth with alpha rarefaction curves, and analyzed for alpha (within-sample) and beta (between-sample) diversity after rarefaction to 48,846 counts.

Stable Iron Isotope (δ^{56}Fe) Analyses

For δ^{56}Fe isotope analysis, 100 mg of each powdered sample was weighed in centrifuge tubes and diluted with 10 ml of 1 M HCl. After mixing, the ferrozine assay was performed to determine the total Fe content following reduction of Fe(III) to Fe(II) with hydroxylammonium chloride (Viollier et al., 2000; Hegler et al., 2008). The absorbance was measured at a wavelength of 562 nm. Based on the Fe concentration measurements, an aliquot of 10 μg Fe per sample was transferred to a perfluoroalkoxy (PFA) beaker and doped with 10 μg of ^{57}Fe-^{58}Fe double spike. For extraction and purification of iron at the Isotope Geochemistry Group's clean-room facility of the University of Tübingen (Germany), Spectra/Chrom polypropylene (PP) columns filled with 1 ml anion exchange resin (DOWEX AG 1 × 8, 100–200 mesh) were used. After cleaning with 2 ml H_2O, followed by 5 ml 5 M HNO_3 and 2 ml H_2O, the resin was conditioned with 5 ml (1 ml, 1 ml, 3 ml in turn) 6 M HCl. Each sample was loaded in 1 ml 6 M HCl onto the columns. Sample matrix elements except Fe were eluted from the resin using an additional 6 ml (1 ml, 1 ml, 4 ml in turn) 6 M HCl. The purified Fe was eluted from the resin with 2 ml (1 ml, 1 ml in turn) H_2O and 4.5 ml (1 ml, 3.5 ml in turn) 5 M HNO_3.

Fe isotope measurements were done on the Thermo Fisher Neptune Plus multicollector inductively coupled plasma mass spectrometer (MC-ICP-MS) of the Isotope Geochemistry Group at the University of Tübingen. High-mass resolution ($\Delta m/m = 10{,}500$) was employed to separate polyatomic isobars from Fe isotopes (mainly $^{40}Ar^{14}N^+$ from $^{54}Fe^+$, $^{40}Ar^{16}O^+$, $^{40}Ar^{17}O^+$ and $^{40}Ar^{18}O^+$ from $^{56}Fe^+$, $^{57}Fe^+$, and $^{58}Fe^+$ respectively), while isobaric interferences from $^{54}Cr^+$ on $^{54}Fe^+$ and $^{58}Ni^+$ on $^{58}Fe^+$ were corrected by monitoring $^{52}Cr^+$ and $^{60}Ni^+$ respectively, assuming natural isotopic composition for chromium and nickel (Wieser et al., 2013). Instrumental mass bias was corrected with the double spike deconvolution method described by Compston and Oversby (1969). The calculation of the δ^{56}Fe isotope values is as follows:

$$\left(\frac{\left(^{56}Fe/^{54}Fe\right)_{\text{sample}}}{\left(^{56}Fe/^{54}Fe\right)_{\text{standard}}}-1\right)\times 1000‰, \qquad (1)$$

where the international reference material IRMM-014 was used as the reference delta-zero standard throughout this study. To ensure δ^{56}Fe data quality, two internal standards, HanFe and TuebFe, were measured together with IRMM-014 (IRMM-014: $0.000‰ \pm 0.016‰$, $n = 14$; long-term average of $0.000‰ \pm 0.034‰$, $n = 313$; HanFe: $0.276‰ \pm 0.021‰$, long-term average of $0.289‰ \pm 0.038‰$, $n = 133$; TuebFe: $-0.385‰ \pm 0.015‰$, long-term average of $-0.377‰ \pm 0.038‰$, $n = 103$). The measured data are within the two standard deviations (2SD) range of all standards and hence considered stable and consistent. Fe concentrations in blanks that were processed in parallel (0.52 ng Fe/g, 0.58 ng Fe/g, 0.89 ng Fe/g, and 0.94 ng Fe/g) were negligible compared to the amount of processed sample iron of 10 μg.

RESULTS

Textural and Mineralogical Features of the Iron Microbialites

The analyzed iron microbialite was ~10 cm thick and characterized by a non-isopachous layering with lateral bifurcation and coalescence of column-like structures (Figs. 1C, 1D, 2A, and 2B). Individual layers were ~1 cm thick and exhibited alternating color and texture (brownish red versus yellowish red, porous versus dense respectively).

All Mössbauer spectra obtained at 77 K exhibited doublets and sextets indicative of different Fe phases. More specifically, the spectra showed a doublet with a center shift (CS) value of 0.48–0.49 mm/s and a quadrupole split (QS) value of 1.17–1.21 mm/s. Additionally, several sextets were observed, with CS values ranging from 0.45 mm/s to 0.56 mm/s, quadrupole shift (ε) values from −0.29 mm/s to −0.02 mm/s, and magnetic field splitting (H) values between 38.0 T and 49.9 T (Table S1 in the Supplemental Material[1]). The fitting parameters of the sextets were characteristic of Fe(III) (oxyhydr)oxides including goethite, which could be identified based on ε values of <−0.10 mm/s (Murad and Cashion, 2004). Other Fe(III) (oxyhydr)oxides such as hematite (Fe_2O_3; typically H values >50 T; Murad and Cashion, 2004), magnetite (Fe_3O_4; typically CS values >0.65 mm/s; Gorski and Scherer, 2010), and ferrihydrite (normally $Fe_5HO_8 \cdot 4H_2O$; generally QS <1 in doublets; Thompson et al., 2025) were not observed (Table S1).

In Mössbauer spectra obtained at 77 K, jarosite can be identified as a doublet with CS values of 0.48–0.49 mm/s and high QS values of 1.17–1.21 mm/s (Eneroth and Koch, 2004). To support our interpretation of this phase as jarosite, we further analyzed the sample from layer 2 at 295 K and 5 K. At 295 K, the sample spectrum displayed only broadened doublets and was best fitted with a phase having CS values of 0.32–0.34 mm/s and QS values of 0.59–1.4 mm/s, characteristic of jarosite. At 5 K, the spectrum only displayed sextets, consistent with jarosite undergoing a magnetic transition between 77 K and 4.2 K. One of the sextets exhibited fitting parameters matching those of jarosite (Table S1; Eneroth and Koch, 2004; Murad and Cashion, 2004).

Another common mineral in Río Tinto is schwertmannite (Amils et al., 2014). In Mössbauer spectra recorded at 295 K and 77 K, at least one Fe(III) doublet of schwertmannite exhibits QS values much lower than those measured in our study (~0.65 mm/s versus >1.19 mm/s, respectively; Thompson et al., 2025). Given this discrepancy, we conclude that schwertmannite was either below the detection limit of Mössbauer spectroscopy (<5%) or absent in our samples.

[1]Supplemental Material. Supplementary mineralogical, geochemical, and molecular genetic data are provided in Tables S1–S4 and Figures S1–S3. Additional Mars-related context is provided in Figure S4. Please visit https://doi.org/10.1130/GSAB.S.32652795 to access the supplemental material; contact editing@geosociety.org with any questions.

Downloaded from http://pubs.geoscienceworld.org/gsa/gsabulletin/article-pdf/doi/10.1130/B38599.1/8045496/b38599.pdf by Universitaetsbibliothek Tuebingen user on 25

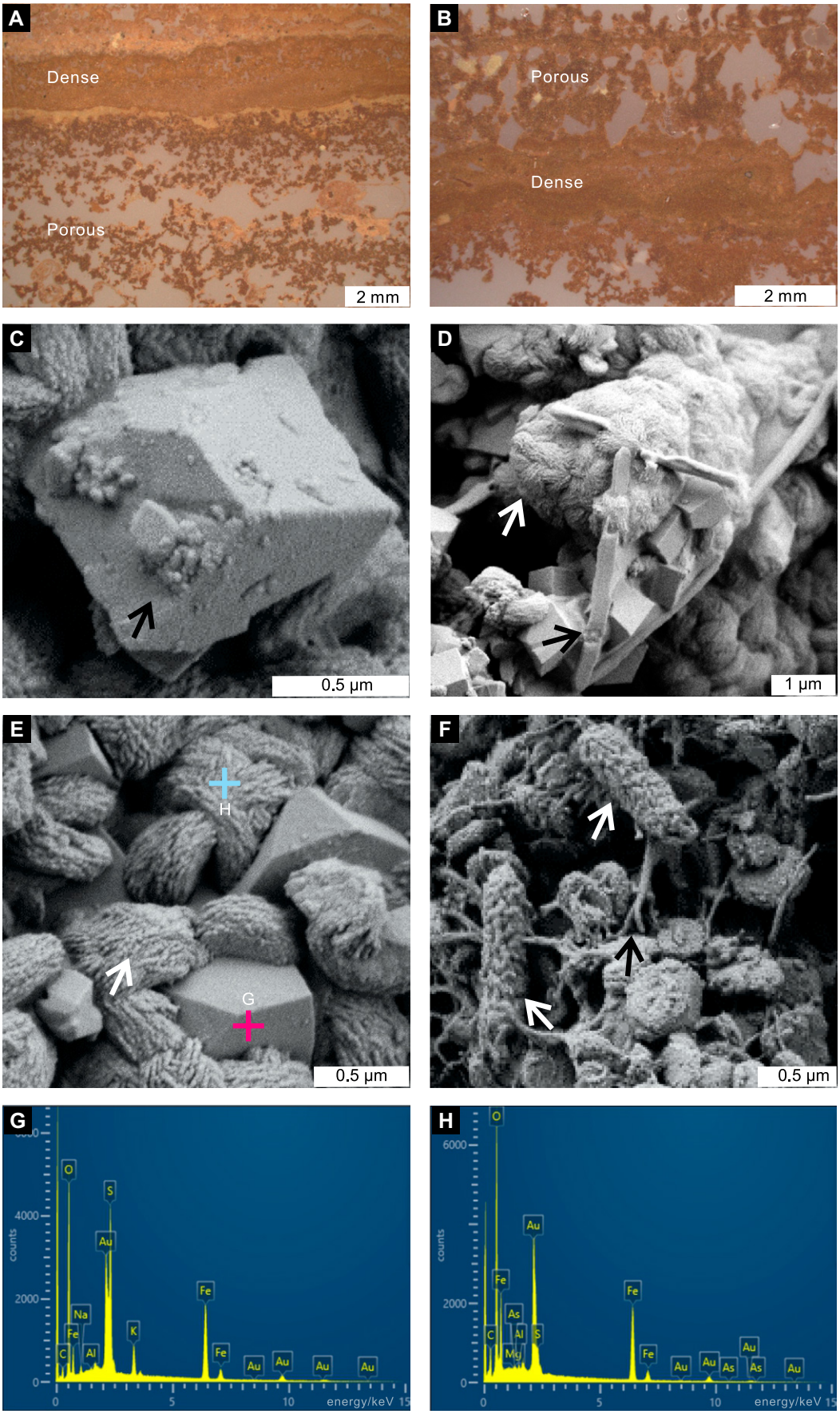

Figure 2. (A, B) Optical photomicrographs (position marked in Fig. 1D) highlighting the difference between dense and porous layers of the iron microbialites. (C–E, G, H) The scanning electron microscope coupled with energy-dispersive X-ray spectroscopy (SEM-EDS) revealed that jarosite occurred as micrometer-scale euhedral crystals (black arrows, C) and goethite as needle-shaped crystals (black arrows, D). These two mineral morphologies were closely associated with Fe(III) (oxyhydr)oxides that appeared pseudo-spherulitic (white arrows, D, E). Au detected in the spectra originates from sample coating. (F) Spatial associations of prokaryotic cells (white arrows), extracellular polymeric substances (EPS; black arrow), and mineral layers.

Downloaded from http://pubs.geoscienceworld.org/gsa/gsabulletin/article-pdf/doi/10.1130/B38599.1/8045496/b38599.pdf by Universitaetsbibliothek Tuebingen user on 25

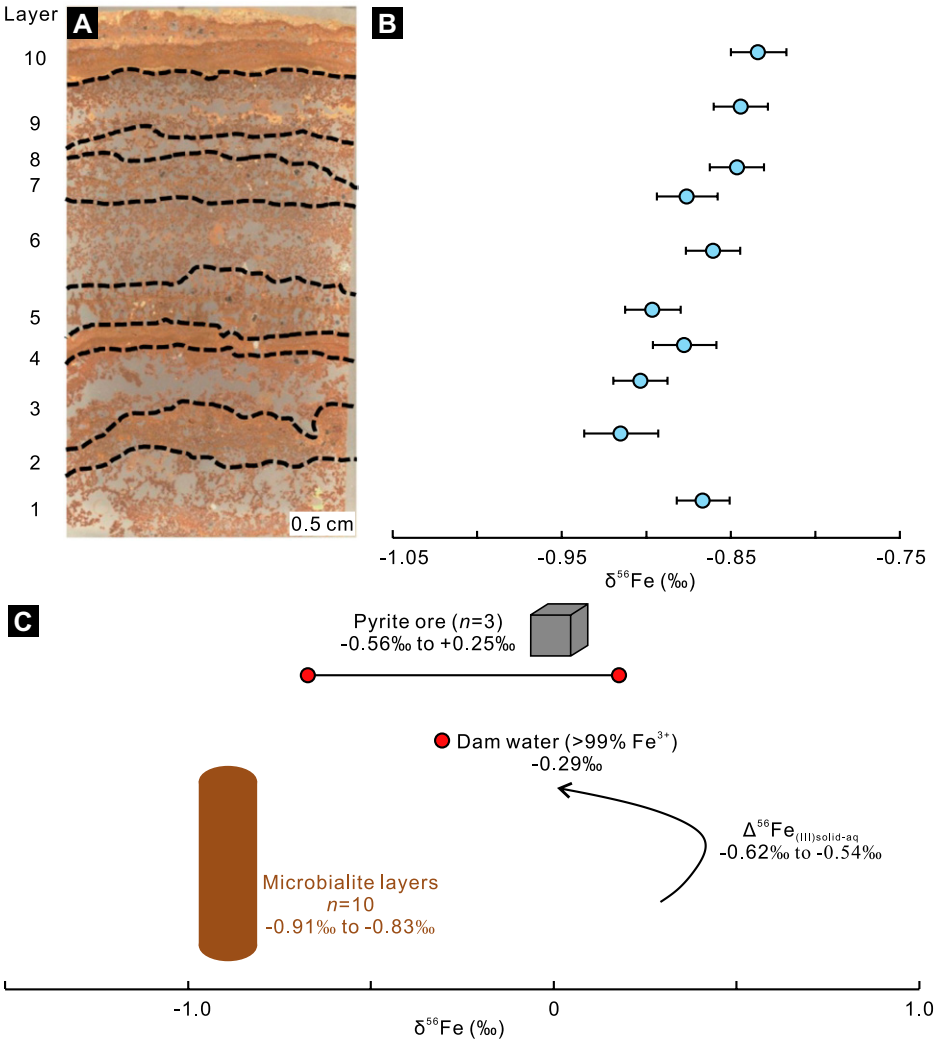

Figure 3. (A, B) δ^{56}Fe values of the different layers of the iron microbialite (−0.91‰ to −0.83‰, −0.87‰ ± 0.016‰ on average, two standard deviations [2SD], $n = 10$). (C) Calculated isotopic differences associated with mineral precipitation ($\Delta^{56}Fe_{(III)solid\text{-}aq}$ = −0.62‰ to −0.54‰) are consistent with the fractionation expected between the observed iron minerals and $Fe^{3+}_{(aq)}$. δ^{56}Fe values for pyrite ore from the Río Tinto are from Egal et al. (2008).

Consistent with Mössbauer spectroscopy, μXRD reflections (goethite: reflections at 24.7° and 42.6° 2θ; jarosite: reflections at 20.8°, 33.7°, and 46.3° 2θ) and Raman indicated that the iron microbialite consisted of jarosite, goethite, and other Fe(III) (oxyhydr)oxides (Figs. 1E and S1A–S1C). Goethite seemed to be less crystalline than jarosite, as indicated by broader μXRD reflections (Fig. S1A; Holder and Schaak, 2019; Ali et al., 2022). Similar features of μXRD reflections indicative of goethite suggested a lower crystallinity in layers with a dense texture than those with a porous texture.

Mössbauer spectra indicated the presence of jarosite (9.2%–23.5%), goethite (31.5%–82.0%), and mixed Fe(III) (oxyhydr)oxides (8.8%–45.0%; Fig. 1E; Table S1). Notably, dense layers (i.e., layers 4, 10) exhibited relatively higher jarosite contents, whereas porous layers (i.e., layers 2, 6, 8) contained relatively higher proportions of goethite (Figs. 1D and 1E). This is consistent with μXRF maps, showing enrichments of S and K tracing jarosite in dense layers (Figs. 1F and S2).

SEM-EDS revealed that jarosite and goethite occurred as μm-scale euhedral and needle-shaped crystals respectively (Fig. 2). These two mineral morphologies were closely associated with Fe(III) (oxyhydr)oxides that appeared pseudo-spherulitic; each "cluster" was ~0.5 μm in size (Figs. 2C–2E, 2G, and 2H). In addition, spatial associations between prokaryotic cells, extracellular polymeric substances (EPS), and minerals were observed by SEM (Fig. 2F). Biomass was present in both dense and porous layers. Prokaryotic cells were relatively dispersed, and EPS were the major constituent of biomass by occurrence.

Stable Iron Isotopes (δ^{56}Fe) of the Iron Microbialites

The acidic reservoir water had ~30 mM dissolved $Fe^{3+}_{(aq)}$ (>99% of total aqueous Fe as determined by ferrozine assay; Hegler et al., 2008). Its δ^{56}Fe value was −0.29‰, consistent with the range reported from pyrite in the area (−0.56‰ to +0.25‰) and water in other parts of the Río Tinto system (−1.76‰ to +0.43‰; Egal et al., 2008). The δ^{56}Fe values of solid phase HCl-extractable Fe from the microbialite layers ranged from −0.91‰ to −0.83‰, with −0.87‰ ± 0.016‰ on average (2SD, $n = 10$; Figs. 3A and 3B; Table S2). The δ^{56}Fe values and layer numbers show a significantly positive correlation (Spearman's rho = 0.756, p = 0.01), indicating an increase of δ^{56}Fe values over depth.

DNA Analyses of the Iron Microbialites

To further investigate the role of microorganisms in the formation of the microbialites, we first analyzed the TOC contents. Generally, dense layers exhibited higher TOC than porous layers, with layer 10 (0.41 ± 0.036 wt%) substantially exceeding layer 6 (0.16 ± 0.004 wt%; Fig. S3; Table S3). Notably, these relatively low TOC values are still ~10 times higher than those measured in situ or expected on Mars (i.e., ~0.03 wt% in the Cumberland mudstone in Gale crater; Stern et al., 2022; Freissinet et al., 2025).

Microbial community analysis based on 16S rRNA indicated a dominance of the archaeal phylum Thermoplasmatota, with lower proportions of the bacterial phyla Pseudomonadota and Actinobacteriota (Fig. 4). Microbial communities in the external (i.e., younger) layers showed a higher diversity (Shannon diversity index, H' = 5.02–5.28), with Thermoplasmatota (28.06%–38.07%) and Pseudomonadota (14.85%–24.70%) being the most prominent, alongside Actinobacteriota (13.03%–16.04%), Deinococcota (3.87%–12.10%), and Chloroflexota (3.73%–8.94%). In contrast, microbial communities in the internal (i.e., older) layers were less diverse (H' = 4.08–4.61), exhibiting a more pronounced dominance of Thermoplasmatota (46.75%–56.45%), followed by Actinobacteriota (17.41%–17.68%) and Chloroflexota (13.62%–16.84%). Pseudomonadota were less prevalent in the internal layers (2.15%–8.73%), which also showed an increase in Nitrospirota (2.01%–5.01%; Fig. 4; Table S4).

Downloaded from http://pubs.geoscienceworld.org/gsa/gsabulletin/article-pdf/doi/10.1130/B38599.1/8045496/b38599.pdf by Universitaetsbibliothek Tuebingen user on 25

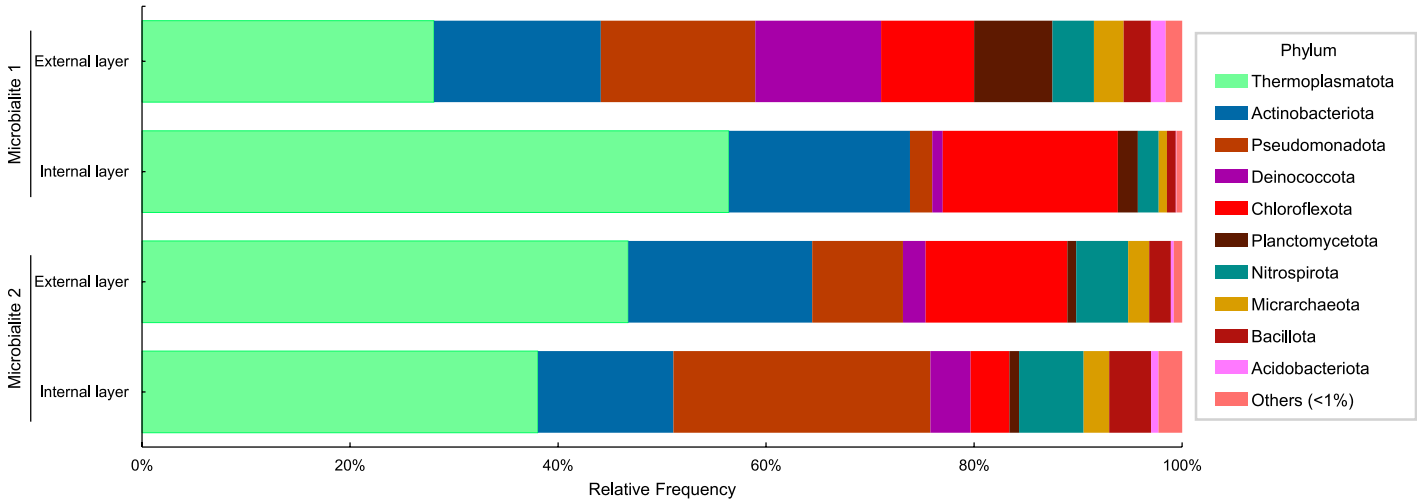

Figure 4. Microbial communities in external and internal layers of two iron microbialites from Río Tinto, Spain, analyzed via DNA-based methods.

DISCUSSION

Iron Microbialite Formation—Microbial vs. Abiotic Processes

Microbial Fe^{2+} oxidation in the Río Tinto subsurface and surface water contributes to its high content of dissolved $Fe^{3+}_{(aq)}$ (Amils et al., 2014, 2023; Abramov et al., 2022). Microbial Fe^{2+} oxidation rates in Río Tinto water, including those of *Acidithiobacillus* and *Leptospirillum* (Abramov et al., 2022), can be 10^5–10^6 times higher than abiotic Fe^{2+} oxidation, which is extremely slow at acidic pH (~2.0; Singer and Stumm, 1970). Notably, in the acidic reservoir water, >99% of total aqueous Fe is dissolved $Fe^{3+}_{(aq)}$. Considering the thickness (~10 cm) and estimated age of the iron microbialite (<100 yrs, based on the age of the reservoir wall), its growth rate must have been at least ~1 mm per year. This precipitation rate is very high considering the slow precipitation kinetics of minerals in the reservoir (Oggerin et al., 2016). Therefore, it is likely that microorganisms contributed to mineral precipitation and, by extension, microbialite formation. Indeed, it was suggested that fungi such as *P. lilacinum* promote Fe(III) mineral formation in the environment by binding metal cations at negatively charged cellular surfaces, resulting in local supersaturation and jarosite precipitation (Oggerin et al., 2016).

The observed community composition of the microbialites as revealed by DNA analyses is distinct from other habitats in Río Tinto. Generally, the microbialite diversity ($H' = 4.08$–5.28) was slightly lower than that in Río Tinto sediments at the estuary ($H' = 5.2$–6.5) but higher than that in the middle course of the acidic river ($H' = 2.65$–3.5; Abramov et al., 2022). More specifically, the main prokaryotes in the water (*Leptospirillum*, *Acidithiobacillus*, and *Acidiphilium*) are much less abundant in the microbialites, while the archaeal phylum Thermoplasmatota is substantially more abundant in the microbialites than in the water (~30%–60% versus >1% respectively; González-Toril et al., 2003). This aligns with previous studies showing the dominance of Thermoplasmatota in anoxic zones of acid mine drainage sites such as Parys Mountain (Wales, UK) and Iron Mountain (California, USA), where it constituted up to 65.5% and 85% of the prokaryotic community respectively (Edwards et al., 2000).

Even though Thermoplasmatota lack rigid cell walls, their activity in the iron-oxidizing cycle can lead to the precipitation of sulfate minerals (e.g., jarosite; Edwards et al., 2000). In addition, related biofilms can trap mineral particles or provide a surface for mineral nucleation, contributing to biomineralization processes and increasing the stability of microbialites (Kish et al., 2016). As in the case of some fungi, the cell walls of bacteria such as Pseudomonadota, Actinobacteriota, and Nitrospirota promote biomineralization by providing surfaces for mineral nucleation, templates for crystal growth, and functional groups for ion binding (Maurice and Warren, 2006). This idea is supported by SEM-EDS analyses of our samples, which revealed spatial associations between prokaryotic cells, EPS, and minerals within the microbialite layers (Fig. 2F). This finding is consistent with previous reports of filamentous Fe(II)-oxidizing bacteria closely associated with iron sulfates and oxides in Río Tinto crusts and sediments (Preston et al., 2011). Hence, eukarya (fungi; Oggerin et al., 2016), archaea (e.g., Thermoplasmatota), and bacteria (e.g., Pseudomonadota, Actinobacteriota, Nitrospirota) could play a crucial role in the formation of jarosite.

After jarosite formation, it may transform into other minerals depending on hydrochemical conditions in the environment, resulting in the alternating color and texture of the iron microbialite layers (Figs. 1C, 1D, 2A, and 2B). These changes may have been driven by seasonal water input (e.g., rainfall), which could have influenced O_2 availability and associated mineral oxidation processes. However, abiotic oxidation of Fe^{2+} by O_2 is extremely slow at low pH (~2.0; Singer and Stumm, 1970). Instead, the observed mineralogical transitions are likely governed by microbial processes. Admixture of freshwater into the acidic reservoir water may cause a slight pH increase, while microbial sulfate or Fe(III) reduction can further elevate pH by consuming SO_4^{2+} or Fe^{3+} respectively, both of which are abundant in Río Tinto (Fig. 4; Table S4). Together, such processes may create transient neutral to alkaline microenvironments (Sánchez-Román et al., 2014). At higher pH, goethite forms preferentially over jarosite (Smith et al., 2006; Ryu and Kim, 2022), a trend also demonstrated in experimental simulations of Martian environments (Mitra et al., 2020; Peretyazhko et al., 2021; Zhang et al., 2024; Mitra, 2025). Thus, goethite formation may have been promoted by jarosite dissolution.

The lower crystallinity of goethite as compared to jarosite in the iron microbialite (e.g., layer 1), as indicated by broader μXRD reflections (Fig. S1A; Ali et al., 2022), is in good accordance with a later formation. The jarosite-goethite transformation sequence also explains

Downloaded from http://pubs.geoscienceworld.org/gsa/gsabulletin/article-pdf/doi/10.1130/B38599.1/8045496/b38599.pdf by Universitaetsbibliothek Tuebingen user on 25

the textural characteristics of the different layers. More specifically, goethite has a significantly lower molar volume than jarosite (21 cm^3/mol versus 160 cm^3/mol, respectively; BRGM Thermoddem database, https://thermoddem.brgm.fr/databases); hence, the transformation of jarosite to goethite should involve a reduction of the mineral volume. Therefore, porous textures can be formed through the (microbially driven) transformation of jarosite to goethite (i.e., jarosite → poorly crystalline Fe(III) (oxyhydr)oxides → goethite).

There have been attempts to employ Fe isotopes as biosignatures because of their large fractionations (Beard et al., 1999; Anbar et al., 2000). Biological involvement in the formation of the iron microbialites is primarily attributed to adsorption or precipitation processes. Indeed, redox reactions such as Fe^{2+} oxidation are not required as the reservoir water already consisted of >99% Fe^{3+}. While redox reactions tend to produce the same isotopic fractionation irrespective of biological or abiotic pathways (Johnson et al., 2020), the adsorption of dissolved Fe to cell surfaces can lead to a clear enrichment of heavy isotopes on the cell surfaces. This process, in turn, leaves behind an isotopically light solution, as shown in culture experiments with cyanobacteria (Mulholland et al., 2015). Given that the adsorption of metal cations at negatively charged cellular surfaces evidently plays a key role in the formation of the analyzed iron microbialites, the latter process needs further investigation. Calculated isotopic differences associated with mineral precipitation ($\Delta^{56}Fe_{(III)solid\text{-}aq} = -0.62‰$ to $-0.54‰$) are consistent with the fractionation expected between the observed iron minerals and $Fe^{3+}_{(aq)}$ (Fig. 3C), with no clear difference in abiotic and biological systems (Balci et al., 2006; Whitworth et al., 2020). For comparison, Fe isotope fractionation in low pH environments of the Ottery Mine in eastern Australia showed a much larger range in $\Delta^{56}Fe_{(III)solid\text{-}aq}$ along the flow-path (~5.2‰; Burton et al., 2022). Thus, Fe isotopes in Río Tinto provide no clear evidence of direct microbial involvement in microbialite formation.

Potential Biosignatures Associated with Iron Microbialites

Several lines of evidence observed in the iron microbialites can be attributed to biological processes: (1) non-isopachous layering, (2) high growth rate, and (3) the presence of microorganisms that likely promote iron mineral precipitation. However, many other features are ambiguous, including mineralogical distribution, TOC contents, and $\delta^{56}Fe$ values. Problematically, high-confidence biosignatures (e.g., microbial cells and DNA; growth rates) cannot be reliably inferred or detected either in the geological record or by Mars rovers, while layered structures can also form abiotically.

Laminated and dome-shaped stromatolite-like structures were also reported from other low pH environments such as the Carnoulès acid mine drainage in France (Leblanc et al., 1996). These deposits consist of abundant poorly crystalline Fe(III) (oxyhydr)oxides, including As-rich schwertmannite (Maillot et al., 2013), and they were found to be associated with living *Thiobacillus*-type bacteria (Leblanc et al., 1996). This is very different to the Río Tinto microbialites analyzed herein, where schwertmannite was below the detection limit of Mössbauer spectroscopy and μXRD or even absent. One possible explanation is a rapid transformation of potential initial schwertmannite to jarosite, perhaps driven by *Acidithiobacillus* (Wang et al., 2006).

The iron microbialites analyzed in this study also exhibited textural and chemical features that are somewhat similar to modern Fe(III) (oxyhydr)oxide deposits observed in deep-sea hydrothermal vent fields in the Norwegian-Greenland Sea (Moeller et al., 2014). More specifically, both deposits consist of centimeter-scale Fe(III) (oxyhydr)oxide layers that are locally porous and show low $\delta^{56}Fe$ values (deposits from hydrothermal vent fields: −2.09‰ to −0.66‰; iron microbialites from Río Tinto: −0.91‰ to −0.83‰). However, in contrast to the Río Tinto microbialites, these deposits formed under circumneutral pH conditions. Considering that Fe(III) (oxyhydr)oxide formation under such conditions can be driven by microaerophilic Fe(II)-oxidizing bacteria (Picard et al., 2015), iron microbialites with similar geologically stable key features may form under conditions different from Río Tinto. This means that iron microbialites not only provide targets for the astrobiological exploration of Mars, but to a wide range of iron-rich environments teeming with prokaryotic life—including ancient hydrothermal sulfide systems, which are widely considered critical for the emergence of prokaryotic life (Martin et al., 2008; Georgieva et al., 2021).

Significance for the Search for Life on Mars

Mars is a prime target for astrobiological studies. Within the next two decades, Martian samples might be returned to Earth (Beaty et al., 2019; Kminek et al., 2022; Hou et al., 2024). Earth-based analog studies are central to the critical analysis of any samples from these missions (Amils et al., 2014; Kaplan et al., 2016; Ruff and Farmer, 2016; Hays et al., 2017; Cavalazzi et al., 2019).

Our results demonstrate that diverse microbial communities flourish under environmental conditions that might have persisted at Meridiani Planum on Mars (Fernández-Remolar et al., 2005). Various prokaryotes in these communities promote the formation of jarosite and Fe(III) (oxyhydr)oxides, such as goethite. Compared to the analyzed microbialites, Meridiani Planum deposits contain higher proportions of jarosite and abundant hematite (Figs. 1E and S4; Fernández-Remolar et al., 2005; Morris et al., 2006). While some of the hematite and jarosite in Meridiani Planum deposits may derive from mineral transformation processes under arid conditions, their Fe(III) (oxyhydr)oxide precursors are thought to have formed under potentially habitable aquatic conditions (Elwood Madden et al., 2004, 2012; Knoll et al., 2005; Barrón et al., 2006; Bibring et al., 2006). It is also important to keep in mind that the formation of Fe(III)-bearing minerals in some regions of Mars can be mediated by a variety of abiotic oxidation processes (e.g., UV rays and reactive chlorine species; Lasne et al., 2016; Mitra et al., 2020; Chan et al., 2025; Viúdez-Moreiras et al., 2025; Mitra, 2025). So far, rover data have not been sufficient for identifying microbial activity in these deposits. Thus, our study reinforces previous recommendations for the return of Meridiani Planum rocks to Earth (Knoll et al., 2005; McSween and Thiemens, 2025).

We have reinforced the utility of layered iron microbialites as a target for the search for life on Mars. However, most individual characteristics analyzed in this study were inconclusive in determining biogenicity. For instance, in situ observable features such as non-isopachous layering can also form abiotically. At the same time, many high-confidence biosignatures associated with the iron microbialites (e.g., microbial cells and DNA, growth rates) cannot be inferred or detected by current Mars rovers. This ambiguity increases the risk of false negatives in extraterrestrial life detection (McMahon and Cosmidis, 2022). To reduce this risk, in situ observable features that qualify rocks for sample return missions must be thoroughly constrained. Crucially, multiple lines of Mars- and Earth-based evidence must then be carefully weighed and integrated into a coherent model that aligns with microbial processes. Learning to use terrestrial analogs to build plausible, testable models is therefore essential for supporting in situ rover missions and sample return campaigns.

ACKNOWLEDGMENTS

We thank S.M. Abramov, M. Bottaro, D. Buchner, T.H. Chiu, C. Dreher, S. Fischer, H. Grimm, L. Grimm, Z. Guo, I. Kleinhanns, J. Nebelsick, V. Nikeleit, B. Nisch, D. Raisch, E. Reitter, F. Schädler,

Downloaded from http://pubs.geoscienceworld.org/gsa/gsabulletin/article-pdf/doi/10.1130/B38599.1/8045496/b38599.pdf by Universitaetsbibliothek Tuebingen user on 25

S. Schafflick, J. Schönig, and Q. Tao for assistance in the research. This study was supported by the National Natural Science Foundation of China (grants 42402128 and 42472371), China Postdoctoral Science Foundation (grant M743291), the University of Tübingen (Baden-Württemberg, Germany; Teach@Tübingen Fellowship), the German Research Foundation (DFG; Emmy Noether Programme, DU 1450/7-1), and the Excellence Strategy of the German Federal and State Governments (Tübingen Structural Microscopy Core Facility). We thank the two anonymous reviewers for their constructive comments, which enhanced the manuscript, and we are grateful to the editors for their handling of the review process.

REFERENCES CITED

Abramov, S.M., Straub, D., Tejada, J., Grimm, L., Schädler, F., Bulaev, A., Thorwarth, H., Amils, R., Kappler, A., and Kleindienst, S., 2022, Biogeochemical niches of Fe-cycling communities influencing heavy metal transport along the Rio Tinto, Spain: Applied and Environmental Microbiology, v. 88, no. 4, https://doi.org/10.1128/aem.02290-21.

Ali, A., Chiang, Y.W., and Santos, R.M., 2022, X-ray diffraction techniques for mineral characterization: A review for engineers of the fundamentals, applications, and research directions: Minerals, v. 12, no. 2, p. 205, https://doi.org/10.3390/min12020205.

Amils, R., Fernández-Remolar, D., and IPBSL Team, 2014, Río Tinto: A geochemical and mineralogical terrestrial analogue of Mars: Life, v. 4, no. 3, p. 511–534, https://doi.org/10.3390/life4030511.

Amils, R., et al., 2023, Coupled C, H, N, S and Fe biogeochemical cycles operating in the continental deep subsurface of the Iberian Pyrite Belt: Environmental Microbiology, v. 25, no. 2, p. 428–453, https://doi.org/10.1111/1462-2920.16291.

Anbar, A.D., Roe, J.E., Barling, J., and Nealson, K.H., 2000, Nonbiological fractionation of iron isotopes: Science, v. 288, no. 5463, p. 126–128, https://doi.org/10.1126/science.288.5463.126.

Andrews, S., 2010, FastQC: A quality control tool for high throughput sequence data: Babraham Bioinformatics: https://www.bioinformatics.babraham.ac.uk/projects/fastqc/ (accessed February 2024).

Arp, G., Reimer, A., and Reitner, J., 2001, Photosynthesis-induced biofilm calcification and calcium concentrations in Phanerozoic oceans: Science, v. 292, no. 5522, p. 1701–1704, https://doi.org/10.1126/science.1057204.

Balci, N., Bullen, T.D., Witte-Lien, K., Shanks, W.C., Motelica, M., and Mandernack, K.W., 2006, Iron isotope fractionation during microbially stimulated Fe(II) oxidation and Fe(III) precipitation: Geochimica et Cosmochimica Acta, v. 70, no. 3, p. 622–639, https://doi.org/10.1016/j.gca.2005.09.025.

Barrón, V., Torrent, J., and Greenwood, J.P., 2006, Transformation of jarosite to hematite in simulated Martian brines: Earth and Planetary Science Letters, v. 251, no. 3–4, p. 380–385, https://doi.org/10.1016/j.epsl.2006.09.022.

Beard, B.L., Johnson, C.M., Cox, L., Sun, H., Nealson, K.H., and Aguilar, C., 1999, Iron isotope biosignatures: Science, v. 285, no. 5435, p. 1889–1892, https://doi.org/10.1126/science.285.5435.1889.

Beaty, D.W., et al., 2019, The potential science and engineering value of samples delivered to Earth by Mars sample return: Meteoritics & Planetary Science, v. 54, no. S1, p. S3–S152, https://doi.org/10.1111/maps.13242.

Bibring, J., et al., 2006, Global mineralogical and aqueous Mars history derived from OMEGA/Mars Express data: Science, v. 312, no. 5772, p. 400–404, https://doi.org/10.1126/science.1122659.

Bolyen, E., et al., 2019, Reproducible, interactive, scalable and extensible microbiome data science using QIIME 2: Nature Biotechnology, v. 37, p. 852–857, https://doi.org/10.1038/s41587-019-0209-9.

Burne, R.V., and Moore, L.S., 1987, Microbialites; organosedimentary deposits of benthic microbial communities: Palaios, v. 2, no. 3, p. 241–254, https://doi.org/10.2307/3514674.

Burton, E.D., Karimian, N., Hamilton, J.L., and Frierdich, A.J., 2022, Iron isotopes in acid mine drainage: Extreme and divergent fractionation between solid (schwertmannite, jarosite, and ferric arsenate) and aqueous species: Environmental Science & Technology, v. 56, no. 24, p. 18,060–18,068, https://doi.org/10.1021/acs.est.2c05999.

Callahan, B.J., McMurdie, P.J., Rosen, M.J., Han, A.W., Johnson, A.J.A., and Holmes, S.P., 2016, DADA2: High-resolution sample inference from Illumina amplicon data: Nature Methods, v. 13, p. 581–583, https://doi.org/10.1038/nmeth.3869.

Caporaso, J.G., et al., 2010, QIIME allows analysis of high-throughput community sequencing data: Nature Methods, v. 7, p. 335–336, https://doi.org/10.1038/nmeth.f.303.

Cavalazzi, B., et al., 2019, The Dallol geothermal area, Northern Afar (Ethiopia)—An exceptional planetary field analog on Earth: Astrobiology, v. 19, no. 4, p. 553–578, https://doi.org/10.1089/ast.2018.1926.

Champenois, F., George, A.D., McNamara, K.J., Shaw, J., and Cherdantseva, M., 2024, Contrasting morphology and growth habits of *Frutexites* in Late Devonian reef complexes of the Canning Basin, northwestern Australia: Geobiology, v. 22, no. 1, https://doi.org/10.1111/gbi.12579.

Chan, Y., Jaeglé, L., Campuzano-Jost, P., Catling, D.C., Furdui, V.I., Jackson, W.A., Jimenez, J.L., Kim, D., and Alexander, B., 2025, Global model of atmospheric chlorate on Earth: Journal of Geophysical Research: Atmospheres, v. 130, no. 5, https://doi.org/10.1029/2024JD042162.

Compston, W., and Oversby, V.M., 1969, Lead isotopic analysis using a double spike: Journal of Geophysical Research, v. 74, no. 17, p. 4338–4348, https://doi.org/10.1029/JB074i017p04338.

da Veiga Leprevost, F., et al., 2017, BioContainers: An open-source and community-driven framework for software standardization: Bioinformatics, v. 33, no. 16, p. 2580–2582, https://doi.org/10.1093/bioinformatics/btx192.

Duda, J.-P., Van Kranendonk, M.J., Thiel, V., Ionescu, D., Strauss, H., Schäfer, N., and Reitner, J., 2016, A rare glimpse of Paleoarchean life: Geobiology of an exceptionally preserved microbial mat facies from the 3.4 Ga Strelley Pool Formation, Western Australia: PLoS One, v. 11, no. 1, https://doi.org/10.1371/journal.pone.0147629.

Edwards, K.J., Bond, P.L., Gihring, T.M., and Banfield, J.F., 2000, An archaeal iron-oxidizing extreme acidophile important in acid mine drainage: Science, v. 287, p. 1796–1799, https://doi.org/10.1126/science.287.5459.1796.

Egal, M., Elbaz-Poulichet, F., Casiot, C., Motelica-Heino, M., Négrel, P., Bruneel, O., Sarmiento, A.M., and Nieto, J.M., 2008, Iron isotopes in acid mine waters and iron-rich solids from the Tinto–Odiel Basin (Iberian Pyrite Belt, Southwest Spain): Chemical Geology, v. 253, no. 3–4, p. 162–171, https://doi.org/10.1016/j.chemgeo.2008.05.006.

Ehlmann, B.L., and Edwards, C.S., 2014, Mineralogy of the Martian surface: Annual Review of Earth and Planetary Sciences, v. 42, p. 291–315, https://doi.org/10.1146/annurev-earth-060313-055024.

Elwood Madden, M.E., Bodnar, R.J., and Rimstidt, J.D., 2004, Jarosite as an indicator of water-limited chemical weathering on Mars: Nature, v. 431, p. 821–823, https://doi.org/10.1038/nature02971.

Elwood Madden, M.E., Madden, A.S., Rimstidt, J.D., Zahrai, S., Kendall, M.R., and Miller, M.A., 2012, Jarosite dissolution rates and nanoscale mineralogy: Geochimica et Cosmochimica Acta, v. 91, p. 306–321, https://doi.org/10.1016/j.gca.2012.05.001.

Eneroth, E., and Koch, C.B., 2004, Fe-hydroxysulphates from bacterial Fe^{2+} oxidation: Hyperfine Interactions, v. 156, no. 1, p. 423–429, https://doi.org/10.1023/B:HYPE.0000043263.25269.2f.

Ewels, P., Magnusson, M., Lundin, S., and Käller, M., 2016, MultiQC: Summarize analysis results for multiple tools and samples in a single report: Bioinformatics, v. 32, no. 19, p. 3047–3048, https://doi.org/10.1093/bioinformatics/btw354.

Fernández-Remolar, D.C., Morris, R.V., Gruener, J.E., Amils, R., and Knoll, A.H., 2005, The Río Tinto Basin, Spain: Mineralogy, sedimentary geobiology, and implications for interpretation of outcrop rocks at Meridiani Planum, Mars: Earth and Planetary Science Letters, v. 240, no. 1, p. 149–167, https://doi.org/10.1016/j.epsl.2005.09.043.

Fraeman, A.A., et al., 2020, Evidence for a diagenetic origin of Vera Rubin Ridge, Gale crater, Mars: Summary and synthesis of *Curiosity*'s exploration campaign: Journal of Geophysical Research: Planets, v. 125, no. 12, https://doi.org/10.1029/2020JE006527.

Freissinet, C., et al., 2025, Long-chain alkanes preserved in a Martian mudstone: Proceedings of the National Academy of Sciences of the United States of America, v. 122, no. 13, https://doi.org/10.1073/pnas.2420580122.

García-Moyano, A., González-Toril, E., Aguilera, A., and Amils, R., 2007, Prokaryotic community composition and ecology of floating macroscopic filaments from an extreme acidic environment, Río Tinto (SW, Spain): Systematic and Applied Microbiology, v. 30, no. 8, p. 601–614, https://doi.org/10.1016/j.syapm.2007.08.002.

Georgieva, M.N., Little, C.T.S., Maslennikov, V.V., Glover, A.G., Ayupova, N.R., and Herrington, R.J., 2021, The history of life at hydrothermal vents: Earth-Science Reviews, v. 217, https://doi.org/10.1016/j.earscirev.2021.103602.

González-Toril, E., Llobet-Brossa, E., Casamayor, E.O., Amann, R., and Amils, R., 2003, Microbial ecology of an extreme acidic environment, the Tinto River: Applied and Environmental Microbiology, v. 69, no. 8, p. 4853–4865, https://doi.org/10.1128/AEM.69.8.4853-4865.2003.

Gorski, C.A., and Scherer, M.M., 2010, Determination of nanoparticulate magnetite stoichiometry by Mössbauer spectroscopy, acidic dissolution, and powder X-ray diffraction: A critical review: American Mineralogist, v. 95, no. 7, p. 1017–1026, https://doi.org/10.2138/am.2010.3435.

Grüning, B., Dale, R., Sjödin, A., Chapman, B.A., Rowe, J., Tomkins-Tinch, C.H., Valieris, R., Köster, J., and The Bioconda Team, 2018, Bioconda: Sustainable and comprehensive software distribution for the life sciences: Nature Methods, v. 15, no. 7, p. 475–476, https://doi.org/10.1038/s41592-018-0046-7.

Hays, L.E., Graham, H.V., Des Marais, D.J., Hausrath, E.M., Horgan, B., McCollom, T.M., Parenteau, M.N., Potter-McIntyre, S.L., Williams, A.J., and Lynch, K.L., 2017, Biosignature preservation and detection in Mars analog environments: Astrobiology, v. 17, no. 4, p. 363–400, https://doi.org/10.1089/ast.2016.1627.

Hazen, R.M., et al., 2023, On the diversity and formation modes of martian minerals: Journal of Geophysical Research: Planets, v. 128, no. 9, https://doi.org/10.1029/2023JE007865.

Hegler, F., Posth, N.R., Jiang, J., and Kappler, A., 2008, Physiology of phototrophic iron(II)-oxidizing bacteria: Implications for modern and ancient environments: FEMS Microbiology Ecology, v. 66, no. 2, p. 250–260, https://doi.org/10.1111/j.1574-6941.2008.00592.x.

Hickman-Lewis, K., et al., 2023, Advanced two- and three-dimensional insights into Earth's oldest stromatolites (ca. 3.5 Ga): Prospects for the search for life on Mars: Geology, v. 51, no. 1, p. 33–38, https://doi.org/10.1130/G50390.1.

Holder, C.F., and Schaak, R.E., 2019, Tutorial on powder X-ray diffraction for characterizing nanoscale materials: American Chemical Society Nano, v. 13, no. 7, p. 7359–7365, https://doi.org/10.1021/acsnano.9b05157.

Hou, Z., et al., 2024, The search for life signatures on Mars by the Tianwen-3 Mars sample return mission: National Science Review, v. 11, no. 11, p. 41–44, https://doi.org/10.1093/nsr/nwae313.

Hurowitz, J.A., et al., 2017, Redox stratification of an ancient lake in Gale crater, Mars: Science, v. 356, no. 6341, https://doi.org/10.1126/science.aah6849.

Johnson, C., Beard, B., and Weyer, S., 2020, Iron Geochemistry: An Isotopic Perspective: Cham, Switzerland, Springer, 360 p., https://doi.org/10.1007/978-3-030-33828-2.

Downloaded from http://pubs.geoscienceworld.org/gsa/gsabulletin/article-pdf/doi/10.1130/B38599.1/8045496/b38599.pdf by Universitaetsbibliothek Tuebingen user on 25

Kaplan, H.H., Milliken, R.E., Fernández-Remolar, D., Amils, R., Robertson, K., and Knoll, A.H., 2016, Orbital evidence for clay and acidic sulfate assemblages on Mars based on mineralogical analogs from Rio Tinto, Spain: Icarus, v. 275, p. 45–64, https://doi.org/10.1016/j.icarus.2016.03.019.

Kish, A., Miot, J., Lombard, C., Guigner, J., Bernard, S., Zirah, S., and Guyot, F., 2016, Preservation of archaeal surface layer structure during mineralization: Scientific Reports, v. 6, https://doi.org/10.1038/srep26152.

Kminek, G., Meyer, M.A., Beaty, D.W., Carrier, B.L., Haltigin, T., and Hays, L.E., 2022, Mars sample return (MSR): Planning for returned sample science: Astrobiology, v. 22, no. S1, p. S-1–S-4, https://doi.org/10.1089/ast.2021.0198.

Knoll, A.H., et al., 2005, An astrobiological perspective on Meridiani Planum: Earth and Planetary Science Letters, v. 240, no. 1, p. 179–189, https://doi.org/10.1016/j.epsl.2005.09.045.

Lagarec, K., and Rancourt, D.G., 1997, Extended Voigt-based analytic lineshape method for determining N-dimensional correlated hyperfine parameter distributions in Mössbauer spectroscopy: Nuclear Instruments and Methods in Physics Research Section B: Beam Interactions with Materials and Atoms, v. 129, no. 2, p. 266–280, https://doi.org/10.1016/S0168-583X(97)00284-X.

Lasne, J., Noblet, A., Szopa, C., Navarro-González, R., Cabane, M., Poch, O., Stalport, F., François, P., Atreya, S.K., and Coll, P., 2016, Oxidants at the surface of Mars: A review in light of recent exploration results: Astrobiology, v. 16, no. 12, p. 977–996, https://doi.org/10.1089/ast.2016.1502.

Leblanc, M., Achard, B., Ben Othman, D., Luck, J.M., Bertrand-Sarfati, J., and Personné, J.Ch., 1996, Accumulation of arsenic from acidic mine waters by ferruginous bacterial accretions (stromatolites): Applied Geochemistry, v. 11, no. 4, p. 541–554, https://doi.org/10.1016/0883-2927(96)00010-8.

Lepot, K., 2020, Signatures of early microbial life from the Archean (4 to 2.5 Ga) eon: Earth-Science Reviews, v. 209, https://doi.org/10.1016/j.earscirev.2020.103296.

Lueders, T., Manefield, M., and Friedrich, M.W., 2004, Enhanced sensitivity of DNA- and rRNA-based stable isotope probing by fractionation and quantitative analysis of isopycnic centrifugation gradients: Environmental Microbiology, v. 6, no. 1, p. 73–78, https://doi.org/10.1046/j.1462-2920.2003.00536.x.

Maillot, F., et al., 2013, Structure and reactivity of As(III)- and As(V)-rich schwertmannites and amorphous ferric arsenate sulfate from the Carnoulès acid mine drainage, France: Comparison with biotic and abiotic model compounds and implications for As remediation: Geochimica et Cosmochimica Acta, v. 104, p. 310–329, https://doi.org/10.1016/j.gca.2012.11.016.

Martin, M., 2011, Cutadapt removes adapter sequences from high-throughput sequencing reads: EMBnet.journal, v. 17, no. 1, p. 10–12, https://doi.org/10.14806/ej.17.1.200.

Martin, W., Baross, J., Kelley, D., and Russell, M.J., 2008, Hydrothermal vents and the origin of life: Nature Reviews Microbiology, v. 6, no. 11, p. 805–814, https://doi.org/10.1038/nrmicro1991.

Maurice, P.A., and Warren, L.A., 2006, Introduction to Geomicrobiology: Microbial Interactions with Minerals, *in* Maurice, P.A., Warren, L.A., Bain, D.C., and Schroeder, P.A., eds., Methods for Study of Microbe-Mineral Interactions: The Clay Minerals Society, CMS Workshop Lectures Series, v. 14, p. 1–35, https://doi.org/10.1346/CMS-WLS-14.1.

McMahon, S., and Cosmidis, J., 2022, False biosignatures on Mars: Anticipating ambiguity: Journal of the Geological Society, v. 179, no. 2, https://doi.org/10.1144/jgs2021-050.

McSween, H.Y., and Thiemens, M.H., 2025, The scientific value of Mars Sample Return: Proceedings of the National Academy of Sciences of the United States of America, v. 122, no. 2, https://doi.org/10.1073/pnas.2415280121.

Mitra, K., 2025, Oxychlorine species on Mars: A review: Reviews of Geophysics, v. 63, no. 4, https://doi.org/10.1029/2024RG000861.

Mitra, K., Moreland, E.L., and Catalano, J.G., 2020, Capacity of chlorate to oxidize ferrous iron: Implications for iron oxide formation on Mars: Minerals, v. 10, no. 9, p. 729, https://doi.org/10.3390/min10090729.

Moeller, K., Schoenberg, R., Grenne, T., Thorseth, I.H., Drost, K., and Pedersen, R.B., 2014, Comparison of iron isotope variations in modern and Ordovician siliceous Fe oxyhydroxide deposits: Geochimica et Cosmochimica Acta, v. 126, p. 422–440, https://doi.org/10.1016/j.gca.2013.11.018.

Morris, R.V., et al., 2006, Mössbauer mineralogy of rock, soil, and dust at Meridiani Planum, Mars: Opportunity's journey across sulfate-rich outcrop, basaltic sand and dust, and hematite lag deposits: Journal of Geophysical Research: Planets, v. 111, no. E12, https://doi.org/10.1029/2006JE002791.

Mulholland, D.S., Poitrasson, F., Shirokova, L.S., González, A.G., Pokrovsky, O.S., Boaventura, G.R., and Vieira, L.C., 2015, Iron isotope fractionation during Fe(II) and Fe(III) adsorption on cyanobacteria: Chemical Geology, v. 400, p. 24–33, https://doi.org/10.1016/j.chemgeo.2015.01.017.

Murad, E., and Cashion, J., 2004, Mössbauer Spectroscopy of Environmental Materials and Their Industrial Utilization: Kluwer Academic Publishers, 417 p., https://doi.org/10.1007/978-1-4419-9040-2.

Noffke, N., 2021, Microbially induced sedimentary structures in clastic deposits: Implication for the prospection for fossil life on Mars: Astrobiology, v. 21, no. 7, p. 866–892, https://doi.org/10.1089/ast.2021.0011.

Oggerin, M., Tornos, F., Rodriguez, N., Pascual, L., and Amils, R., 2016, Fungal iron biomineralization in Río Tinto: Minerals, v. 6, no. 2, https://doi.org/10.3390/min6020037.

Pei, Y., Suarez-Gonzalez, P., Duda, J.-P., and Reitner, J., 2024, Organic matter influence on ooid formation: New insights into classic examples (Great Salt Lake, USA; Triassic Germanic Basin, Germany): Sedimentology, v. 71, no. 5, p. 1419–1435, https://doi.org/10.1111/sed.13179.

Peretyazhko, T.S., Ming, D.W., Morris, R.V., Agresti, D.G., and Buckley, W.P., 2021, Formation of Fe(III) (hydr)oxides from Fe(II) sulfides: Implications for akaganeite detection on Mars: ACS Earth and Space Chemistry, v. 5, no. 8, p. 1934–1947, https://doi.org/10.1021/acsearthspacechem.1c00075.

Picard, A., Kappler, A., Schmid, G., Quaroni, L., and Obst, M., 2015, Experimental diagenesis of organo-mineral structures formed by microaerophilic Fe(II)-oxidizing bacteria: Nature Communications, v. 6, 6277, https://doi.org/10.1038/ncomms7277.

Planavsky, N., Rouxel, O., Bekker, A., Shapiro, R., Fralick, P., and Knudsen, A., 2009, Iron-oxidizing microbial ecosystems thrived in late Paleoproterozoic redox-stratified oceans: Earth and Planetary Science Letters, v. 286, no. 1–2, p. 230–242, https://doi.org/10.1016/j.epsl.2009.06.033.

Preston, L.J., Shuster, J., Fernández-Remolar, D., Banerjee, N.R., Osinski, G.R., and Southam, G., 2011, The preservation and degradation of filamentous bacteria and biomolecules within iron oxide deposits at Rio Tinto, Spain: Geobiology, v. 9, no. 3, p. 233–249, https://doi.org/10.1111/j.1472-4669.2011.00275.x.

Quast, C., Pruesse, E., Yilmaz, P., Gerken, J., Schweer, T., Yarza, P., Peplies, J., and Glöckner, F.O., 2013, The SILVA ribosomal RNA gene database project: Improved data processing and web-based tools: Nucleic Acids Research, v. 41, no. D1, p. D590–D596, https://doi.org/10.1093/nar/gks1219.

Reinhardt, M., et al., 2024, Aspects of the biological carbon cycle in a ca. 3.42-billion-year-old marine ecosystem: Precambrian Research, v. 402, https://doi.org/10.1016/j.precamres.2024.107289.

Ruff, S.W., and Farmer, J.D., 2016, Silica deposits on Mars with features resembling hot spring biosignatures at El Tatio in Chile: Nature Communications, v. 7, https://doi.org/10.1038/ncomms13554.

Ryu, J., and Kim, Y., 2022, Mineral transformation and dissolution of jarosite coprecipitated with hazardous oxyanions and their mobility changes: Journal of Hazardous Materials, v. 427, https://doi.org/10.1016/j.jhazmat.2022.128283.

Sánchez España, J., Santofimia Pastor, E., and López Pamo, E., 2007, Iron terraces in acid mine drainage systems: A discussion about the organic and inorganic factors involved in their formation through observations from the Tintillo acidic river (Riotinto mine, Huelva, Spain): Geosphere, v. 3, no. 3, p. 133–151, https://doi.org/10.1130/GES00069.1.

Sánchez-Román, M., Fernández-Remolar, D., Amils, R., Sánchez-Navas, A., Schmid, T., Martin-Uriz, P.S., Rodríguez, N., McKenzie, J.A., and Vasconcelos, C., 2014, Microbial mediated formation of Fe-carbonate minerals under extreme acidic conditions: Scientific Reports, v. 4, https://doi.org/10.1038/srep04767.

Singer, P.C., and Stumm, W., 1970, Acidic mine drainage: The rate-determining step: Science, v. 167, p. 1121–1123, https://doi.org/10.1126/science.167.3921.1121.

Smith, A.M.L., Hudson-Edwards, K.A., Dubbin, W.E., and Wright, K., 2006, Dissolution of jarosite $[KFe_3(SO_4)_2(OH)_6]$ at pH 2 and 8: Insights from batch experiments and computational modelling: Geochimica et Cosmochimica Acta, v. 70, no. 3, p. 608–621, https://doi.org/10.1016/j.gca.2005.09.024.

Stern, J.C., et al., 2022, Organic carbon concentrations in 3.5-billion-year-old lacustrine mudstones of Mars: Proceedings of the National Academy of Sciences of the United States of America, v. 119, no. 27, https://doi.org/10.1073/pnas.2201139119.

Straub, D., Blackwell, N., Langarica-Fuentes, A., Peltzer, A., Nahnsen, S., and Kleindienst, S., 2020, Interpretations of environmental microbial community studies are biased by the selected 16S rRNA (gene) amplicon sequencing pipeline: Frontiers in Microbiology, v. 11, https://doi.org/10.3389/fmicb.2020.550420.

Suarez-Gonzalez, P., Benito, M.I., Quijada, I.E., Mas, R., and Campos-Soto, S., 2019, 'Trapping and binding': A review of the factors controlling the development of fossil agglutinated microbialites and their distribution in space and time: Earth-Science Reviews, v. 194, p. 182–215, https://doi.org/10.1016/j.earscirev.2019.05.007.

Thompson, A., Byrne, J.M., Dreher, C.L., Grigg, A.R.C., Joshi, P., Latta, D.E., Neumann, A., Notini, L., O'Neill, K.E.B., and Rothwell, K.A., 2025, Current practices for analyzing soils and sediments via Mössbauer spectroscopy: Journal of Plant Nutrition and Soil Science, v. 188, no. 5, p. 742–773, https://doi.org/10.1002/jpln.12024.

Tice, M.M., and Lowe, D.R., 2004, Photosynthetic microbial mats in the 3,416-Myr-old ocean: Nature, v. 431, p. 549–552, https://doi.org/10.1038/nature02888.

Valantinas, A., et al., 2025, Detection of ferrihydrite in Martian red dust records ancient cold and wet conditions on Mars: Nature Communications, v. 16, 1712, https://doi.org/10.1038/s41467-025-56970-z.

Van Kranendonk, M.J., 2011, Morphology as an Indictor of Biogenicity for 3.5–3.2 Ga Fossil Stromatolites from the Pilbara Craton, Western Australia, *in* Reitner, J., Quéric, N., and Arp, G., eds., Advances in Stromatolite Geobiology: Springer, Berlin, Heidelberg, Lecture Notes in Earth Sciences, v. 131, p. 537–554, https://doi.org/10.1007/978-3-642-10415-2_32.

Viollier, E., Inglett, P.W., Hunter, K., Roychoudhury, A.N., and Van Cappellen, P., 2000, The ferrozine method revisited: Fe(II)/Fe(III) determination in natural waters: Applied Geochemistry, v. 15, no. 6, p. 785–790, https://doi.org/10.1016/S0883-2927(99)00097-9.

Viúdez-Moreiras, D., Zorzano, M., Lemmon, M.T., Fairén, A.G., Saiz-Lopez, A., and Smith, M.D., 2025, Ultraviolet and biological effective dose observations at Gale Crater, Mars: Proceedings of the National Academy of Sciences of the United States of America, v. 122, no. 21, https://doi.org/10.1073/pnas.2426611122.

Wang, H., Bigham, J.M., and Tuovinen, O.H., 2006, Formation of schwertmannite and its transformation to jarosite in the presence of acidophilic iron-oxidizing microorganisms: Materials Science and Engineering: C, v. 26, no. 4, p. 588–592, https://doi.org/10.1016/j.msec.2005.04.009.

Weimann, L., et al., 2024, Carbonaceous matter in ~3.5 Ga black bedded barite from the Dresser Formation

Downloaded from http://pubs.geoscienceworld.org/gsa/gsabulletin/article-pdf/doi/10.1130/B38599.1/8045496/b38599.pdf by Universitaetsbibliothek Tuebingen user on 25

(Pilbara Craton, Western Australia)—Insights into organic cycling on the juvenile Earth: Precambrian Research, v. 403, https://doi.org/10.1016/j.precamres.2024.107321.

Westall, F., et al., 2015, Biosignatures on Mars: What, where, and how? Implications for the search for martian life: Astrobiology, v. 15, no. 11, p. 998–1029, https://doi.org/10.1089/ast.2015.1374.

Whitworth, A.J., Brand, H.E.A., and Frierdich, A.J., 2020, Iron isotope exchange and fractionation between jarosite and aqueous Fe(II): Chemical Geology, v. 554, https://doi.org/10.1016/j.chemgeo.2020.119802.

Wieser, M.E., et al., 2013, Atomic weights of the elements 2011 (IUPAC Technical Report): Pure and Applied Chemistry, v. 85, p. 1047–1078, https://doi.org/10.1351/PAC-REP-13-03-02.

Zhang, L., Fu, X., Ling, Z., Shi, E., and Cao, H., 2024, The coprecipitation of akaganeite and jarosite and its implications for the late-stage diagenetic fluids in the Vera Rubin Ridge, Gale crater, Mars: Journal of Geophysical Research: Planets, v. 129, no. 4, https://doi.org/10.1029/2023JE008157.

Science Editor: Troy Rasbury
Associate Editor: Gregory Henkes

Manuscript Received 15 June 2025
Revised Manuscript Received 12 March 2026
Manuscript Accepted 1 June 2026

Downloaded from http://pubs.geoscienceworld.org/gsa/gsabulletin/article-pdf/doi/10.1130/B38599.1/8045496/b38599.pdf by Universitaetsbibliothek Tuebingen user on 25